PERGAMON

International Journal of Heat and Mass Transfer 44 (2001) 99–110

International Journal of HEAT and MASS TRANSFER

www.elsevier.com/locate/ijhmt

Numerical simulation of the stability of steadily cooled flowing layer

K.M. Moon, T.H. Song*

Department of Mechanical Engineering, Korea Advanced Institute of Science and Technology, Kusong-dong, Yusong-gu, Taejon 305-701 South Korea

Received 21 May 1999; received in revised form 23 February 2000

Abstract

Initiation of longitudinal roll cell convection in a fully developed, steadily cooled flowing layer has been investigated. The upper free surface is subject to convective cooling and the rigid bottom is insulated. The critical Rayleigh number and the associated wavenumber are obtained as functions of the Prandtl number, the dimensionless mass flow rate of main flow and the Biot number at the upper surface. Linear stability theory is not valid in this case. The SIMPLER algorithm with periodic boundary condition is used to directly simulate the flow field numerically in an unsteady manner. In the region of steady bifurcation, the critical Rayleigh number is significantly greater than the results using the linear stability theory. However, when the Prandtl number is greater than 10, the linear stability theory is asymptotically valid, and the critical Rayleigh number and the associated wavenumber are very close to the results from the linear stability theory. Oscillatory motion, or Hopf bifurcation, occurs when the Prandtl number is less than 0.1. © 2000 Published by Elsevier Science Ltd.

1. Introduction

Product quality of glass, steel and many other industrial materials is significantly affected by melting, refining and forming processes. Raw molten material undergoes cooling and heating during these processes. Thermal instability often arises when the bottom is warmer than the upper surface. It appears when the temperature difference between upper and bottom layers is greater than a certain critical value and/or the fluid layer is sufficiently deep. When it occurs, the flow pattern and the thermal behavior are significantly altered, which may eventually change the product quality beyond control. It is thus very important to find the stability limits in those processes.

This paper examines the stability of a steadily cooled flowing layer. Fig. 1 shows the schematic of the problem. This type of flow is frequently found in the forehearth of glass production lines, and in the continuous casting of steel. The temperatures of fluid layer and environment constantly decrease along the main flow direction. The upper boundary is free and the lower boundary is rigid. The fluid layer is cooled by environmental convection at the upper surface and insulated at the lower surface. This unstable temperature profile may alter the flow pattern completely. However, as long as the instability is suppressed, the fully developed velocity profile is maintained as w_s, as shown in Fig. 1. The steady temperature profile is also depicted as T_s. When the instability takes places, convective roll cells of certain pattern appear in the layer. The stability

* Corresponding author. Tel.: +82-42-869-3032; fax: +82-42-869-3210.

E-mail address: thsong@sorak.kaist.ac.kr (T.H. Song).

0017-9310/01/$ - see front matter © 2000 Published by Elsevier Science Ltd.
PII: S0017-9310(00)00108-3

Nomenclature

a	the wavenumber, $= 2\pi H/L$
Bi	the Biot number, $= hH/k$
C	steady cooling speed (K/m)
g	gravitational acceleration (9.81 m/s^2)
H	depth of the fluid layer
h	heat transfer coefficient
k	thermal conductivity
L	spanwise period length
M	dimensionless mass flow rate, $= \dot{m}/\rho_0\alpha$
$\dot{m}$	mass flow rate per unit depth (kg/s m)
Pr	the Prandtl number, $= \nu/\alpha$
p	pressure
Ra	the Rayleigh number, $= g\beta CH^4/\alpha\nu$
Ra_m	the modified Rayleigh number, $= Ra(\theta_b-\theta_u)$
T	temperature
t	time
u	x-direction velocity
v	y-direction velocity
w	z-direction velocity
x, z	horizontal coordinates
y	vertical coordinate

Greek symbols

α	thermal diffusivity
β	volumetric thermal expansion coefficient
ϕ	general dependent variable
φ	inclination angle of the bed
ν	kinematic viscosity
θ	dimensionless temperature, $= T_1/CH$
ρ	density

Subscripts

b	bottom surface
cr	critical value
new	present iteration value
0	reference
old	previous iteration value
r	real
s	initial state
u	upper surface
∞	surrounding

Superscripts

$'$	perturbed quantity
$*$	dimensionless quantity

limit is dependent on the pattern of roll cells. The pattern which initiates at the lowest Rayleigh number is not completely known yet. de Graaf et al. [1], though, find the occurrence of the roll cells whose axes are parallel to the main flow direction in the experiment of natural convection of inclined channel. Such roll cells are shown in Fig. 1. Since this pattern is shown to occur in that similar case, we limit ourselves to this roll cell pattern in this paper and scrutinize the stability limit.

Many researchers have reported about the instability of natural convection. A confined fluid layer heated from below has been studied by Pellew and Southwell [2] analytically. Sparrow et al. [3] study a similar pro-

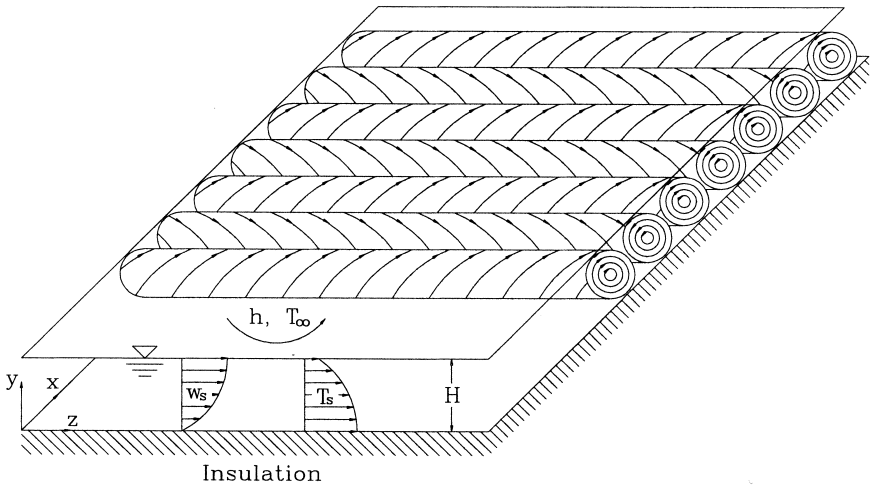

Fig. 1. Schematic of the steadily cooled flowing layer.

blem heated by uniform heat source. The effect of radiative heating is also investigated by Yang [4]. Maekawa and Abe [5] report the effect of electric field on the initiation of natural convection in a confined fluid layer, while Pearson [6] investigates the effect of surface tension in the same problem. All these researches are suited to analytical approach since their problems allow the application of linear stability theory [2]. When this theory does not hold, as is frequent in the case of low Prandtl number flow, the conservation equations of mass, momentum and energy need be solved directly in an unsteady manner to allow steady oscillatory flow as well as the exponential instability growth. Chao et al. [7] report the dependence of the flow instability on the Prandtl number. Their results show that the linear stability theory is not valid for low Prandtl number flows. Lee et al. [8] report linearized stability of fluid flowing over a heated plate. Song [9], on the other hand, reports his results of the current problem applying the method of Pellew and Southwell [2]. Song's results are based on the linear stability theory and need be examined carefully since it is known to be applicable for high Prandtl number fluids only [7].

This study employs a numerical simulation. Unsteady, three-dimensional momentum and energy equations are reduced to two-dimensional equations after some modifications. And, these equations are solved as a substitution for the linear stability theory. Periodic boundary conditions are used to describe the roll cell motion. The analysis is made using a SIMPLER-based code. The onset of roll cell is summarized through the critical Rayleigh number and the associated wavenumber. The results are compared with Song's linear results [9].

2. Problem definition, formulation and numerical scheme

In the present problem, the flow is assumed to be incompressible and the fluid properties are assumed to be constant. The continuity, momentum and energy equations are written as follows:

$$\frac{\partial u}{\partial x}+\frac{\partial v}{\partial y}+\frac{\partial w}{\partial z}=0, \tag{1}$$

$$\frac{\partial u}{\partial t}+u\frac{\partial u}{\partial x}+v\frac{\partial u}{\partial y}+w\frac{\partial u}{\partial z} =-\frac{1}{\rho}\frac{\partial p_{\mathrm{r}}}{\partial x}+\nu\left(\frac{\partial^2 u}{\partial x^2}+\frac{\partial^2 u}{\partial y^2}+\frac{\partial^2 u}{\partial z^2}\right), \tag{2}$$

$$\frac{\partial v}{\partial t}+u\frac{\partial v}{\partial x}+v\frac{\partial v}{\partial y}+w\frac{\partial v}{\partial z} =-\frac{1}{\rho}\frac{\partial p_{\mathrm{r}}}{\partial y}+\nu\left(\frac{\partial^2 v}{\partial x^2}+\frac{\partial^2 v}{\partial y^2}+\frac{\partial^2 v}{\partial z^2}\right)-g, \tag{3}$$

$$\frac{\partial w}{\partial t}+u\frac{\partial w}{\partial x}+v\frac{\partial w}{\partial y}+w\frac{\partial w}{\partial z} =-\frac{1}{\rho}\frac{\partial p_{\mathrm{r}}}{\partial z}+\nu\left(\frac{\partial^2 w}{\partial x^2}+\frac{\partial^2 w}{\partial y^2}+\frac{\partial^2 w}{\partial z^2}\right)+g\sin\varphi, \tag{4}$$

$$\frac{\partial T}{\partial t}+u\frac{\partial T}{\partial x}+v\frac{\partial T}{\partial y}+w\frac{\partial T}{\partial z} =\alpha\left(\frac{\partial^2 T}{\partial x^2}+\frac{\partial^2 T}{\partial y^2}+\frac{\partial^2 T}{\partial z^2}\right). \tag{5}$$

In Eq. (4), the effect of slight inclination angle φ of the bed is included. However, the angle is so small that $\cos\varphi$ is virtually unity as has been implicitly taken in Eq. (3). The lower and upper boundary conditions are given as follows:

$$u=0,\quad v=0,\quad w=0,\quad \frac{\partial T}{\partial y}=0 \tag{6}$$

at the lower surface.

$$\frac{\partial u}{\partial y}=0,\quad v=0,\quad \frac{\partial w}{\partial y}=0,\quad -k\frac{\partial T}{\partial y}=h(T-T_\infty) \tag{7}$$

at the upper surface,

where T_∞ is the surrounding temperature. We assume that the temperatures of the fluid layer and surrounding gas above the upper surface decrease at a constant rate along the z-axis so that,

$$T(x,y,z)=T_1(x,y)-Cz+T_0, \tag{8}$$

where C is the temperature gradient along the z-axis. Note that T_∞ also decreases with gradient C. The reference temperature T_0 may be taken arbitrarily. We choose T_0 as T_∞ at $z=0$ to simplify the equations to follow.

The Boussinesq approximation is applied, i.e., density is assumed to be constant except in the buoyancy term in the vertical direction. The density is linearized using a reference temperature T_0,

$$\rho=\rho_0\left[1-\beta(T-T_0)\right]. \tag{9}$$

Then the real pressure p_{r} is expressed as

$$p_r(x, y, z) = p(x, y) + p_\infty + \int_y^H \rho_0 g(1 + \beta C z)\, dy, \quad (10)$$

where p_∞ is the environmental pressure (constant), ρ_0 is a reference density of the fluid and H is the vertical depth. Note that p_r increases along the z-axis since the density increases by lowered temperature.

Velocities u, v are initially zero in Eq. (4) so that for w_s,

$$0 = -\frac{1}{\rho_0}\frac{\partial p_r}{\partial z} + \nu\frac{\partial^2 w_s}{\partial y^2} + g\sin\varphi. \quad (11)$$

As w_s is fully developed, it is independent of x and z. Then H is not changed along the z-axis. The pressure gradient along the z-axis can be obtained by directly differentiating the real pressure,

$$-\frac{\partial p_r}{\partial z} = -\rho_0 g\beta C(H - y). \quad (12)$$

Introducing this expression in Eq. (11),

$$\nu\frac{\partial^2 w_s}{\partial y^2} = g\beta C(H - y) - g\sin\varphi. \quad (13)$$

The w_s-velocity field is obtained by integrating Eq. (13) and defining mass flow rate per unit spanwise depth as $\dot{m} = \int_0^H \rho_0 w_s\, dy$,

$$w_s = \frac{g\beta C H^3}{\nu}\left[-\frac{1}{6}\left(\frac{y}{H}\right)^3 + \frac{5}{16}\left(\frac{y}{H}\right)^2 - \frac{1}{8}\frac{y}{H}\right] + \frac{\dot{m}}{\rho_0 H}\left[-\frac{3}{2}\left(\frac{y}{H}\right)^2 + 3\frac{y}{H}\right]. \quad (14)$$

Comparing Eqs. (11) and (14), the pressure gradient can be replaced as,

$$-\frac{1}{\rho_0}\frac{\partial p_r}{\partial z} + g\sin\varphi = g\beta C H\left(\frac{y}{H} - \frac{5}{8}\right) + 3\frac{\nu\dot{m}}{\rho_0 H^3}. \quad (15)$$

The pressure gradients along the x- and y-axis can be obtained by directly differentiating the real pressure. Therefore, using Eqs. (8) and (9),

$$-\frac{\partial p_r}{\partial x} = -\frac{\partial p}{\partial x},$$

$$-\frac{\partial p_r}{\partial y} - \rho g = -\frac{\partial p}{\partial y} + \rho_0 g\beta T_1. \quad (16)$$

We further assume that this expression of w-momentum driving forces is not changed at the early stage of instability occurrence. It means that $w \cong w_s$, $w \gg u$ and $w \gg v$ so that Eq. (4) can be linearized without losing accuracy. We substitute Eqs. (8), (15) and (16) into Eqs. (1)–(5). They are nondimensionalized as follows:

$$\frac{\partial u^*}{\partial x^*} + \frac{\partial v^*}{\partial y^*} = 0, \quad (17)$$

$$\frac{\partial u^*}{\partial t^*} + u^*\frac{\partial u^*}{\partial x^*} + v^*\frac{\partial u^*}{\partial y^*} = -\frac{\partial p^*}{\partial x^*} + Pr\left(\frac{\partial^2 u^*}{\partial x^{*2}} + \frac{\partial^2 u^*}{\partial y^{*2}}\right), \quad (18)$$

$$\frac{\partial v^*}{\partial t^*} + u^*\frac{\partial v^*}{\partial x^*} + v^*\frac{\partial v^*}{\partial y^*} = -\frac{\partial p^*}{\partial y^*} + Pr\left(\frac{\partial^2 v^*}{\partial x^{*2}} + \frac{\partial^2 v^*}{\partial y^{*2}}\right) + RaPr\theta, \quad (19)$$

$$\frac{\partial w^*}{\partial t^*} + u^*\frac{\partial w^*}{\partial x^*} + v^*\frac{\partial w^*}{\partial y^*} = Pr\left(\frac{\partial^2 w^*}{\partial x^{*2}} + \frac{\partial^2 w^*}{\partial y^{*2}}\right) + RaPr\left(y^* - \frac{5}{8}\right) + 3PrM, \quad (20)$$

$$\frac{\partial \theta}{\partial t^*} + u^*\frac{\partial \theta}{\partial x^*} + v^*\frac{\partial \theta}{\partial y^*} = \frac{\partial^2 \theta}{\partial x^{*2}} + \frac{\partial^2 \theta}{\partial y^{*2}} + w^*. \quad (21)$$

Note that the z-axis is eliminated for this roll cell pattern. The dimensionless quantities are defined as:

$$t^* = \frac{t}{H^2/\alpha}, \quad x^* = \frac{x}{H}, \quad y^* = \frac{y}{H}, \quad p^* = \frac{p}{\rho_0\alpha^2/H^2}, \quad u^* = \frac{u}{\alpha/H}, \quad v^* = \frac{v}{\alpha/H}, \quad w^* = \frac{w}{\alpha/H}, \quad \theta = \frac{T_1}{CH}, \quad Pr = \frac{\nu}{\alpha}, \quad Ra = \frac{g\beta C H^4}{\alpha\nu} \quad \text{and} \quad M = \frac{\dot{m}}{\rho_0\alpha}. \quad (22)$$

The initial conditions of velocities are given as the steady flow:

$$u_s^* = 0, \quad v_s^* = 0, \quad w_s^* = Ra\left(-\frac{1}{6}y^{*3} + \frac{5}{16}y^{*2} - \frac{1}{8}y^*\right) + M\left(-\frac{3}{2}y^{*2} + 3y^*\right). \quad (23)$$

The thermal initial condition is obtained from Eqs. (21) and (23),

$$\theta_s = Ra\left(\frac{1}{120}y^{*5} - \frac{5}{192}y^{*4} + \frac{1}{48}y^{*3} - \frac{1}{320}\right) + M\left(\frac{1}{8}y^{*4} - \frac{1}{2}y^{*3} + \frac{3}{8}\right) + \frac{M}{Bi}, \quad (24)$$

where the Biot number is defined as $Bi = hH/k$. In Eqs. (23) and (24), the first terms on the right-hand side represent the effect of adverse pressure gradient due to cooling while the other terms show the effect of steady through-flow.

The lower and upper boundary conditions are given as follows:

$$u^* = 0, \quad v^* = 0, \quad w^* = 0, \quad \frac{\partial\theta}{\partial y^*} = 0 \quad (25)$$

at the lower surface.

$$\frac{\partial u^*}{\partial y^*} = 0, \quad v^* = 0, \quad \frac{\partial w^*}{\partial y^*} = 0, \quad \frac{\partial\theta}{\partial y^*} = -Bi\theta \quad (26)$$

at the upper surface.

Periodic boundary conditions are used at the spanwise boundaries (i.e., at $x^* = 0$ and L^*). The flow configuration given in Fig. 1 illustrates the periodic motion well, i.e., the velocity and temperature fields repeat itself spanwise over every period length L^*. Consequently, the velocity components, pressure and temperature exhibit a periodic behavior [10]:

$$\phi(x^*, y^*) = \phi(x^* + L^*, y^*) = \phi(x^* + 2L^*, y^*) = \cdots, \quad (27)$$

where ϕ represents any dimensionless dependent variable and L^* is a dimensionless period length L/H. The wavenumber a is defined as $a = 2\pi H/L$.

The governing equations are solved in primitive variables in two-dimensional staggered grid based on the control volume method [11]. A uniform grid (40×20) is taken after some verification to be shown later. The QUICK scheme [12] is used in the finite difference formulation of the convective terms to minimize the numerical diffusion. The SIMPLER algorithm [11] is employed to solve the coupled heat transfer and fluid flow. The cyclic tridiagonal matrix algorithm [13] is adopted in x-direction to handle the periodic boundary conditions. The governing equations are solved iteratively at each time step until the solutions are converged. Unsteady scheme is made on a fully implicit method. The steady solution is introduced as the initial condition. No artificial perturbation is needed since the small round-off errors naturally function as disturbances. The employed dimensionless time steps are proportional to $(\Delta x^*)^2/Pr$; they are of the order of 10^{-2}, 10^{-3} and 10^{-4} corresponding to the Prandtl number 0.1, 1 and 10, respectively. The error associated with the time step is made minimal by confirming that even finer time step does not significantly change the numerical results. At each time step, it is necessary to ensure the convergence. The temperature and w^*-velocity convergence criteria are taken as follows:

$$\max\left|\frac{\theta_{new} - \theta_{old}}{\theta_{new}}\right| < 1.0 \times 10^{-6},$$

$$\max\left|\frac{w^*_{new} - w^*_{old}}{w^*_{new}}\right| < 1.0 \times 10^{-6}, \quad (28)$$

where subscripts 'new' and 'old' denote the present and the previous iteration values, respectively. The maximum dimensionless mass imbalance over a control volume is also checked. When converged, the value is maintained to be less than 10^{-6}.

When the upper surface is steadily cooled, the highest temperature appears at the bottom and the lowest temperature appears at the upper surface. Therefore, the Rayleigh number is considered to be better expressed using the modified Rayleigh number Ra_m,

$$Ra_m = Ra(\theta_b - \theta_u), \quad (29)$$

where θ_b and θ_u denote the values of θ_s at the lower and the upper surfaces, respectively. Note that Ra_m is nothing but the most conventional definition of Rayleigh number with flow depth and the temperature difference between the upper and the lower surfaces.

By examining the flow field at a modified Rayleigh number and a wavenumber, we check if a roll cell has taken place or not. The parameters are the Prandtl number, the dimensionless mass flow rate M and the Biot number. The critical Rayleigh number Ra_{cr} is the smallest modified Rayleigh number at which the roll cells first appear. Variables u^*, v^*, $w^* - w^*_s$ and $\theta - \theta_s$ increase with time when the roll cells occur ($Ra_m > Ra_{cr}$) while in the other cases ($Ra_m < Ra_{cr}$), they decrease to zero. At $Ra_m = Ra_{cr}$, these variables remain constant. The critical Rayleigh number is obtained by further varying the wavenumber. The lowest modified Rayleigh number and the associated wavenumber are called the critical Rayleigh number (Ra_{cr}) and the critical wavenumber (a_{cr}), respectively.

We next check the numerical errors. Grid dependence is first examined. The well-known problem of Benard convection with upper free and lower rigid boundaries is used to examine the grid dependence. The calculated results using reduced grids are compared with those using a 100×50 mesh. After some trials, errors of u^*, v^* and θ using 40×20 mesh are found to be less than 1.5%. Compromising between the computational cost and the accuracy, the 40×20

mesh is considered to be appropriate. To further verify the grid, the obtained critical Rayleigh number and the wavenumber are compared with the exact values by Drazin [14]. The exact Ra_{cr} (=1101) and a_{cr} (=2.682) are reproduced almost perfectly by the current numerical scheme. The relative errors of the critical Rayleigh number and the wavenumber are usually less than 1%. Thus, the errors of Ra_{cr} and a_{cr} hereafter are estimated to be less than 1%.

In the actual computations, the CRAY Y-MP C916/

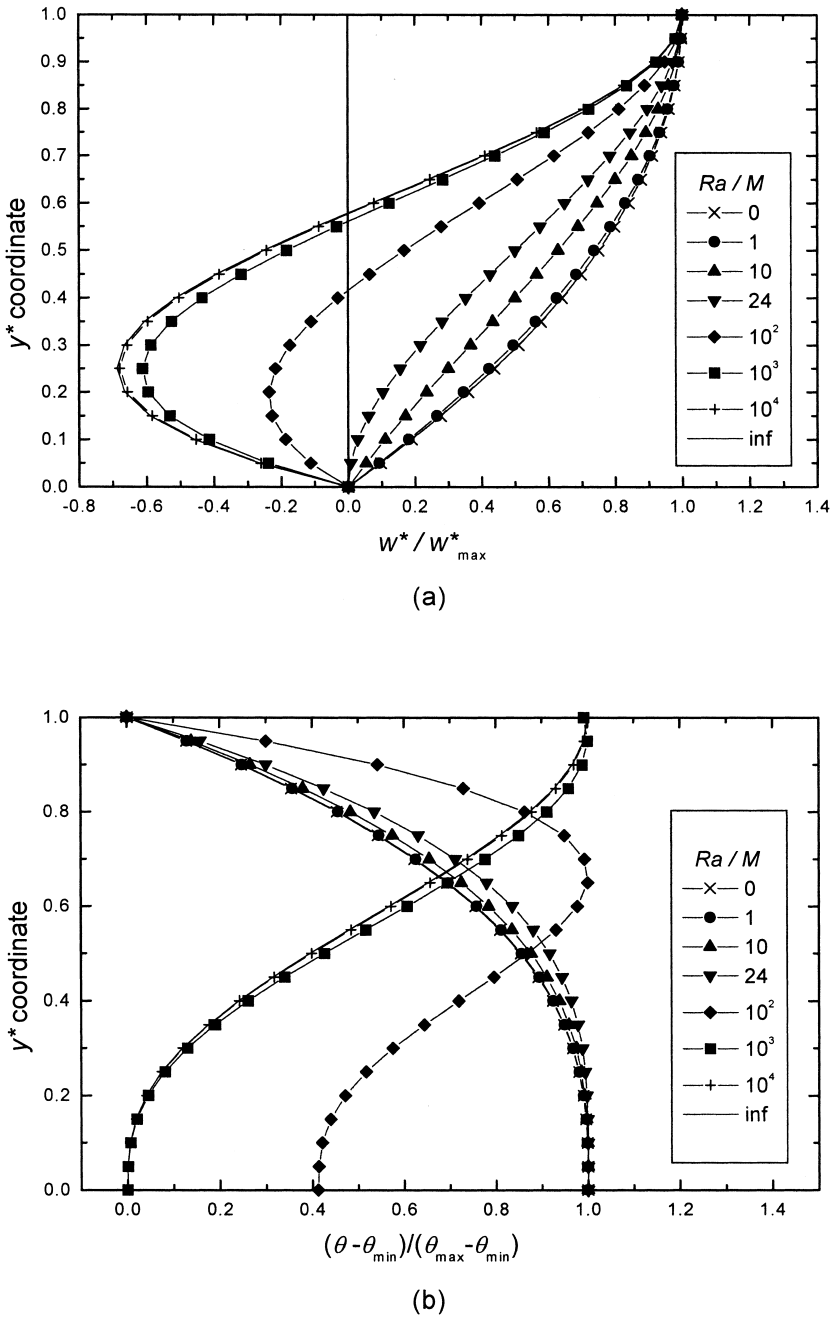

Fig. 2. Initial condition for various Ra/M: (a) w^*-velocity, (b) temperature.

16512 supercomputer has been used. The computation time depends on the Prandtl number, the dimensionless mass flow rate and the Biot number. This time is about 5900 s for a typical set of these three parameters.

The effects of the Prandtl number, the dimensionless mass flow rate and the Biot number are investigated in depth in this study. Fig. 2(a) shows the initial w^*-velocity distribution, and Fig. 2(b) shows the initial temperature distribution. From Fig. 2(a), back flow occurs in the lower part in some cases. It happens when the adverse pressure gradient associated with Ra in Eq. (23) is significantly large compared with the through-flow associated with M. When it happens, material at the end of production line returns along the back flow. This is certainly an abnormal situation induced by an excessive cooling. To avoid the back flow, the w_s^*-velocity gradient at lower surface (see Eq. (23)) must be

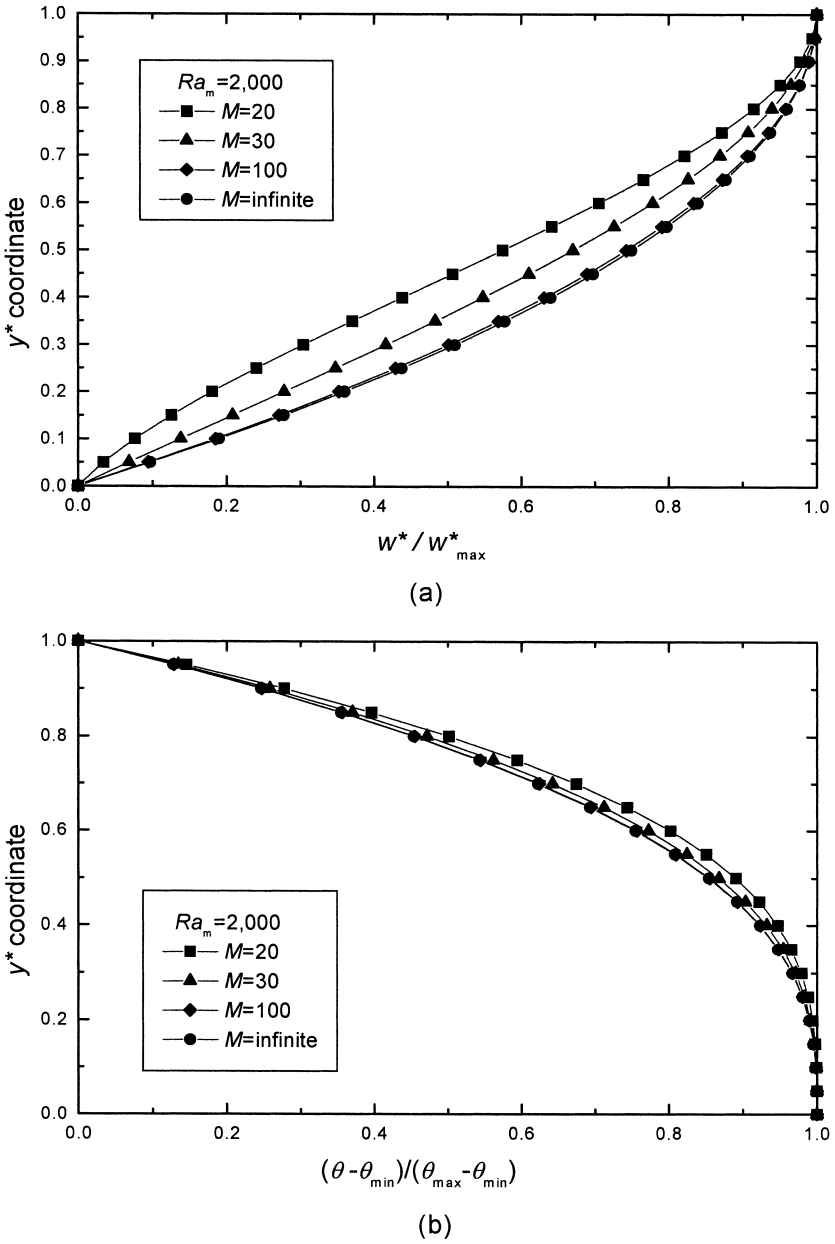

Fig. 3. Initial condition for $Ra_m = 2000$: (a) w^*-velocity, (b) temperature.

greater than 0. This condition is met when

$$\frac{Ra}{M} < 24. \tag{30}$$

When Ra/M is greater than 24, roll cells in the yz-plane occur at the steady state and the maximum initial temperature appears either at the upper surface or in the fluid layer. When it is less than 24, roll cells in the xy-plane may occur and the maximum initial temperature appears at the bottom. As mentioned earlier, we limit ourselves to the roll cells in xy-plane. It is found from Fig. 2 that the flow field and the temperature distribution do not vary significantly with change of Ra/M when the above condition is met, i.e., when the effect of through-flow is dominant. It can also be found from Eq. (24) that,

$$\theta_b - \theta_u = \frac{3}{8}M\left(1 - \frac{Ra}{120M}\right). \tag{31}$$

This is approximately $3M/8$ when $Ra/M < 24$. Introducing Eq. (31) into Eq. (30), we find

$$\frac{Ra_m}{M^2} < 7.2. \tag{32}$$

To investigate the effect of mass flow rate, we vary M to 20, 30 and 100. Fig. 3(a) and (b) show the initial w^*-velocity and initial temperature distribution, respectively. The temperature gradient at the bottom is zero and the highest temperature appears there and the lowest temperature appears at the upper surface. The effect of through-flow is considered to be more important than the effect of adverse pressure gradient due to cooling as M is large. At the limiting case ($M = \infty$), the effect of through-flow is most dominant. The results for $M = 100$ are expected to be almost similar to this limiting case. The Prandtl number is varied from 0.1 to 1 and then to 10 to check the effect.

3. Results and discussions

When the modified Rayleigh number is greater than the critical value, roll cells in the xy-plane occur. Fig. 4 shows an example. The perturbed quantities w' and θ' are $w^* - w_s^*$ and $\theta - \theta_s$, respectively. The magnitudes

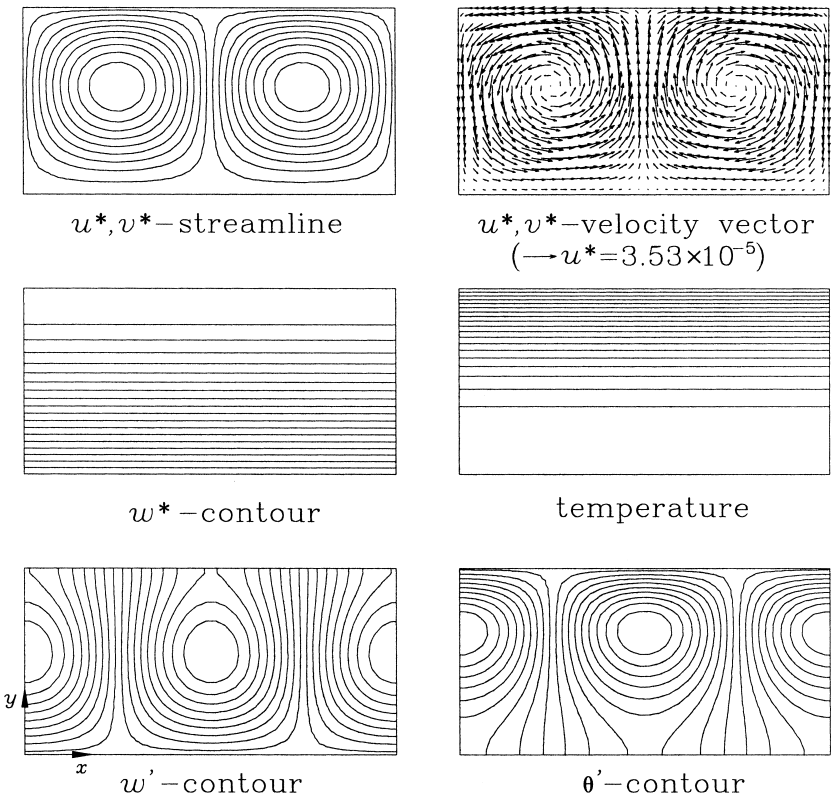

Fig. 4. Velocity and temperature profile of the fluid layer in xy-plane ($Pr = 1$, $M = 30$, $Bi = 1000$, $a = 3.2$, $Ra_m = 1472$).

of u^*, v^*, w' and θ' are of the order of 10^{-6} when divided by the magnitudes of w_s^* and θ_s. It justifies the simplification of $\partial p_r/\partial z$ in Eq. (20). The lower part is initially hot. Two rolls rotate in opposite directions. The w^*-velocity certainly indicates three-dimensional feature of the flow. If the modified Rayleigh number is less than its critical value, initial state ($u^* = v^* = 0$) is maintained.

Fig. 5 shows the critical Rayleigh number and the associated wavenumber when the Prandtl number is 1 and 10. Due to computational difficulty in convergence, we do not calculate the case when the Biot number is less than 3. These results are compared with those of Song [9] which are based on the linear stability theory [2]. Fig. 5(a) and (b) show a_{cr} and Ra_{cr} when the Prandtl number is 1. The critical Rayleigh number and the associated wavenumber increase with decreasing M. Increase in M means increase in flow rate. When it is doubled in a process, the cooling load is also doubled to maintain the same temperature gradient. This may be realized either by increasing h (thus, the Biot number) or by reducing T_∞ (at the same Biot number). In any case, the critical Rayleigh number changes only slightly as can be found from the figure. Since $Ra_m \approx 3RaM/8$ from Eq. (31), Ra_m is almost doubled when M is doubled. Thus, Ra_m may be closer or even greater than the critical Rayleigh number, now resulting in greater instability. The changes of the critical Rayleigh number and the associated wavenumber from $M = 30$ to $M = 100$ are much smaller than those from $M = 20$ to $M = 30$.

Fig. 5(c) and (d) show the critical Rayleigh number and the associated wavenumber when the Prandtl number is 10. The critical numbers show similar behavior as when the Prandtl number is 1, however, they are much smaller than that of $Pr = 1$. Interpretation of the physical consequence requires caution, however. If the viscosity, and thus Pr too, is reduced to 1/10 while the other parameters are the same, then we have 10 times as large modified Rayleigh number ($\approx 3RaM/8$). Note that the steady temperature profile and velocity profile are not altered. The critical Rayleigh number is increased to some degree but it is far below 10 times. Therefore, the modified Rayleigh number is now

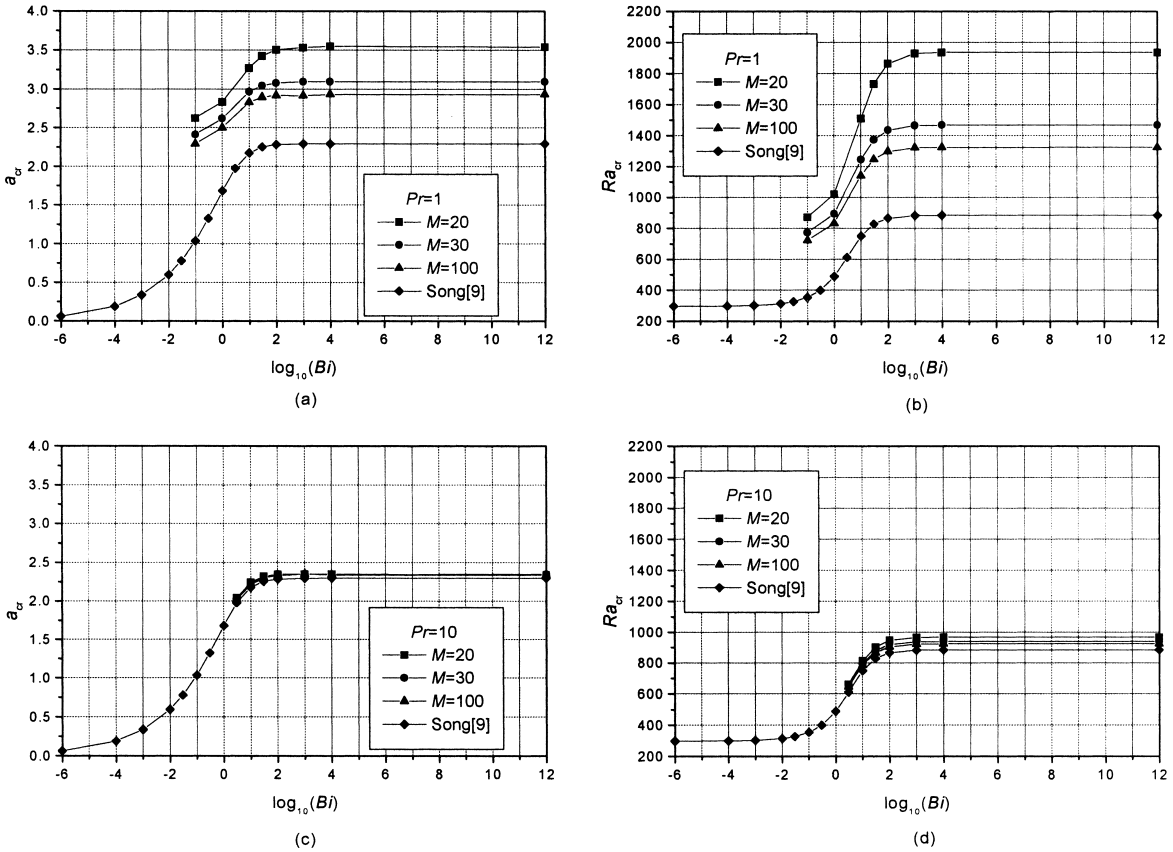

Fig. 5. The critical Rayleigh number and the associated wavenumber: (a) the critical wavenumber ($Pr = 1$), (b) the critical Rayleigh number ($Pr = 1$), (c) the critical wavenumber ($Pr = 10$), (d) the critical Rayleigh number ($Pr = 10$).

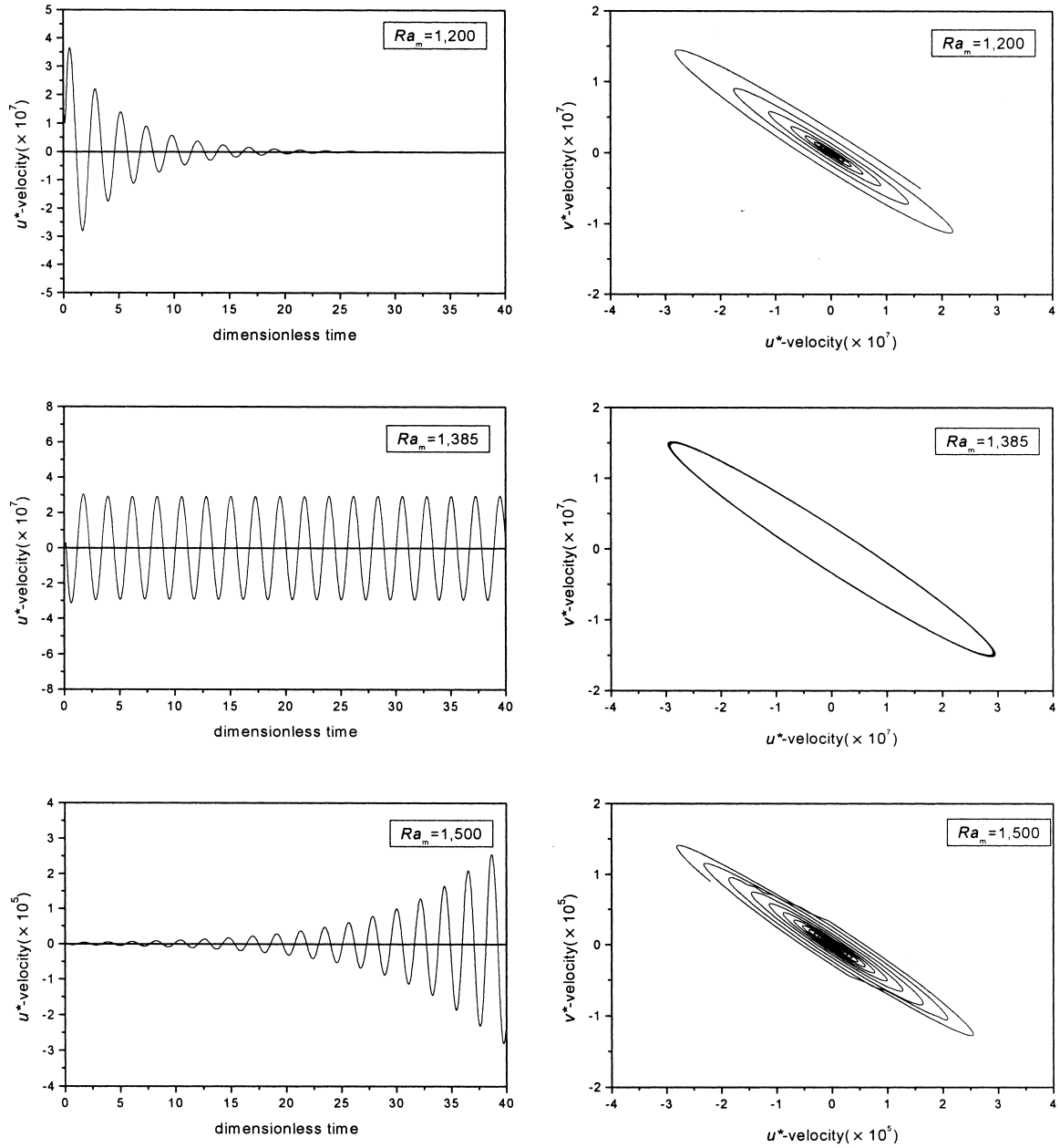

Fig. 6. Transient responses of the u^*-, v^*-velocity at $x^* = 0.11$ and $y^* = 0.11$ ($Pr = 0.1$, $M = 100$, $Bi = 10$, $a = 3$).

closer to the critical Rayleigh number, which means it is less stable. Change of thermal conductivity, on the other hand, is more complicated. Not only Ra_m but also M and Bi are inversely proportional to it. If it is increased 10 times so that Pr changes from 10 to 1, M and Bi are reduced to 1/10; the overall effect results in decrease in the critical Rayleigh number, but not to 1/10. Consequently, Ra_m ($\approx 3RaM/8$) becomes much smaller than the critical Rayleigh number, making the flow more stable. Increase in Pr by the above two manipulations of fluid properties results in opposite consequences in flow stability. The results are in accordance with our physical intuition that greater viscosity or greater thermal conductivity means greater rigidity to the boundary values thus greater stability.

The critical numbers for $Pr = 10$ are almost identi-

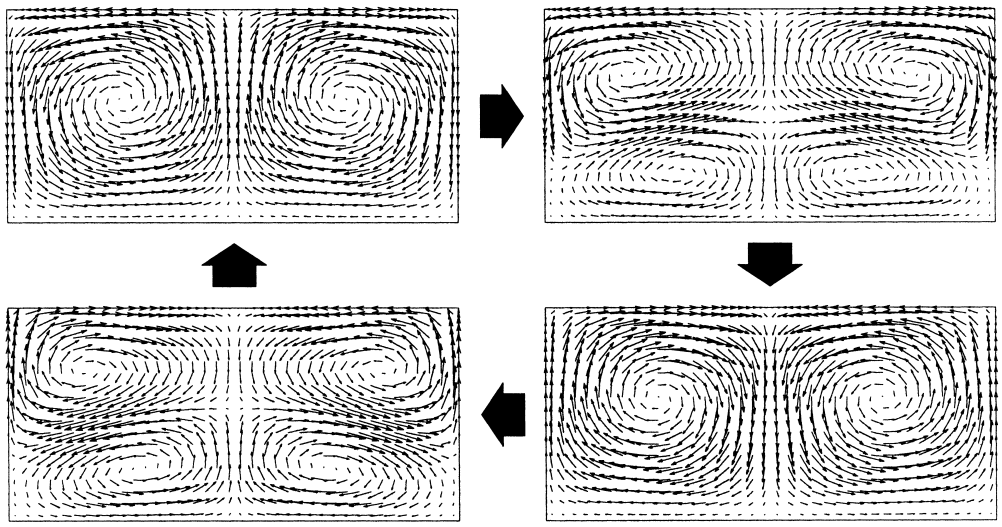

Fig. 7. A series of instantaneous velocity vector during a period for low Prandtl number ($Pr = 0.1$, $M = 100$, $Bi = 10$, $a = 3$, $Ra_m = 1385$).

cal to the results of Song [9], as he solves the current problem using the linear stability theory [2]. The reason of the agreement is considered as follows: Chao et al. [7] reaches the conclusion that convective terms in the momentum equations ($u^*\partial u^*/\partial x^*$, etc.) become negligible compared with the viscous terms ($Pr\partial^2 u^*/\partial x^{*2}$, etc.) for large Prandtl number from their numerical simulation of Benard convection. In this limiting case, the linear stability theory is asymptotically valid when the convective terms in the momentum equations are neglected.

The critical Rayleigh number and the associated wavenumber increase with increasing Biot number. The two critical numbers are very sensitive to the change in the Biot number near $Bi = 1$. When the Biot number is greater than 100, the two critical numbers have nearly constant values. Results for large Bi indicates that large heat transfer coefficient at the upper surface tends to fix the upper surface temperature to the environment temperature, and thus, stabilizes the steady flow. When the Biot number is less than 0.01, the critical Rayleigh number is nearly constant for even smaller Bi according to Song's results. This case actually corresponds to constant heat flux boundary condition.

As can be seen from Fig. 2, the warm (and thus unstable) layer is thicker than the linear temperature profile for $Ra/M < 24$. From Fig. 5(d), the critical Rayleigh number for $M = 100$ and $Bi \cong \infty$ is about 900. When we remember that the Rayleigh-instability case shows $Ra_{cr} = 1101$, we can find that our case shows a more unstable result.

When the modified Rayleigh number is less than 650 for $Bi \geq 3$ and $Pr \geq 1$, the fluid layer is always stable for any Pr, M and Bi. This fact is very informative in industrial applications since below this modified Rayleigh number, the flow is steady and stable, and thus, accurate control of flowing molten product is possible. In terms of the original Rayleigh number defined in Eq. (22), this condition corresponds to

$$Ra \leq \frac{1733}{M}. \tag{33}$$

When the Prandtl number is as small as 0.1, velocities and temperature are found to oscillate at all combinations of M and Bi, and over fairly wide variation of a. Extremely long computing time is needed to simulate the oscillatory motion. It is beyond practical possibility to find the critical Rayleigh number. So, we only calculate a typical case ($Pr = 0.1$) and plot the result in Fig. 6. If the modified Rayleigh number is taken as 1385, velocities and temperature oscillate with uniform amplitude. On the other hand, these amplitudes converge to 0 or diverge to ∞ when the modified Rayleigh number is less or greater than 1385 as shown in Fig. 6. This type of bifurcation is called Hopf bifurcation. When it occurs, the flow changes from steady ($u^* = v^* = 0$) to oscillatory behavior. Velocities u^* and v^* change the flow direction during the oscillation. This means oscillatory change in cell patterns. Fig. 7 shows u^* and v^* velocities during one period of time. The dimensionless period time is 2.08. Initially, two rolls rotate in the opposite direction with upward flow at the center and then the rolls change the direction. The reason why oscillatory bifurcation appears with small Prandtl number is not clear. The most we can infer is

that the perturbed velocities exhibit fairly large inertia for low Pr as has been reasoned by Chao et al. [7]. It can then skip the steady bifurcation stage and directly transfer to oscillatory motion. The concrete border of Hopf bifurcation on the Pr, Bi and M is not found, though.

4. Conclusion

The stability limits of longitudinal roll cells in a steadily cooled flowing layer without back current are investigated using an unsteady SIMPLER code with a periodic boundary condition for $Bi \geq 3$. Steady two-dimensional roll cells appear when $Pr \geq 1$. In this case, the critical Rayleigh number based on the lower and upper surface temperature difference and the associated wavenumber increase with decreasing Pr, increasing Bi and decreasing M. If the Prandtl number is greater than 10, the two critical numbers may be obtained using the linear stability theory as they are not dependent on the Prandtl number any more. The critical Rayleigh number has nearly uniform values when the Biot number is greater than 100 or smaller than 0.01. The fluid layer is found stable for any Pr (≥ 1), M and Bi (≥ 3) when the modified Rayleigh number is smaller than 650. Hopf bifurcation is found to occur when the Prandtl number is as small as 0.1, though the exact regime and the critical Rayleigh number are not obtained.

References

[1] J.G.A. de Graaf, E.F.M. van der Held, The relation between the heat transfer and the convection phenomena in enclosed plane air layers, Applied Scientific Research Series A 3 (1953) 393–409.

[2] A.R. Pellew, R.V. Southwell, On maintained convective motion in a fluid heated from below, Proc. R. Soc. Series A 176 (1940) 312–343.

[3] E.M. Sparrow, R.J. Goldstein, V.K. Jonsson, Thermal instability in a horizontal layer: effect of boundary conditions and non-linear temperature profile, Journal of Fluid Mechanics 18 (1964) 513–528.

[4] W.M. Yang, Thermal instability of a fluid layer induced by radiation, Numerical Heat Transfer Part A 17 (1990) 365–376.

[5] T. Maekawa, K. Abe, Onset of natural convection under electric field, in: J.R. Lloyd, Y. Kurosaki (Eds.), Proceedings of the ASME/JSME Thermal Engineering Joint Conference 1, Reno, Nevada, 1991, pp. 17–24.

[6] J.R.A. Pearson, On convection cells induced by surface tension, Journal of Fluid Mechanics 4 (1958) 489–500.

[7] P. Chao, S.W. Churchill, H. Ozoe, The dependence of the critical Rayleigh number on the Prandtl number, in: J. Zierep, H. Oertel Jr. (Eds.), Convective Transport and Instability Phenomena, Braun, Karlsruhe, 1982, pp. 55–70.

[8] H.R. Lee, T.S. Chen, B.F. Armaly, Non-parallel thermal instability of forced convection flow over a heated non-isothermal horizontal flat plate, International Journal of Heat and Mass Transfer 33 (9) (1990) 2019–2028.

[9] T.H. Song, Y.T. Han, K.O. Lim, Initiation of natural convection in a steadily cooled flowing layer, in: Proceedings of International Seminar on Mathematical Simulation in the Glass Melting, Horni Becva, Czech Pepublic, 1995, pp. 1–10.

[10] S.V. Patankar, C.H. Liu, E.M. Sparrow, Fully developed flow and heat transfer in ducts having streamwise-periodic variations of cross-sectional area, Journal of Heat Transfer 99 (1977) 180–186.

[11] S.V. Patankar, Numerical Heat Transfer and Fluid Flow, Hemisphere, New York, 1980.

[12] B.P. Leonard, A stable and accurate convective modelling procedure based on quadratic upstream interpolation, Computer Methods in Applied Mechanics and Engineering 19 (1979) 59–98.

[13] J.H. Ahlberg, E.N. Nilson, J.L. Walsh, The Theory of Splines and Their Applications, Academic Press, New York, 1967.

[14] P.G. Drazin, W.H. Reid, Hydrodynamic Stability, Cambridge University Press, Cambridge, 1981, p. 52.